Infrared Spectroscopy of a Small Ion Solvated by Helium: OH Stretching Region of He_N-$HOCO^+$

Julia A. Davies,[1] Nicholas A. Besley,[2] Shengfu Yang,[1] and Andrew M. Ellis[1,a)]

[1] Department of Chemistry, University of Leicester, University Road, Leicester, LE1 7RH, UK

[2] School of Chemistry, University of Nottingham, University Park, Nottingham, NG7 2RD, UK

[a)] Electronic mail: andrew.ellis@le.ac.uk

Manuscript submitted to *J. Chem. Phys.*

The Journal of Chemical Physics

ABSTRACT

Messenger spectroscopy is a well-established method for recording infrared (IR) spectra of molecular ions. It relies upon the tagging of weakly bound atoms or molecules, known as the 'messenger', to the ion of interest. The ideal tag species is helium since it has the weakest possible interaction with any molecular ion and is consequently the least likely to alter their structure and function. However the attachment of a helium tag is challenging because of the exceptionally cold conditions that are inherently required. In this work, electron ionization of doped liquid helium nanodroplets has been used to create cations tagged with a variable number (N) of helium atoms. Mass-selective ion detection has made it possible to record IR spectra as a function of N, thus revealing the effect on the structure and charge distribution within the ionic core as solvation becomes more extensive. We illustrate this capability for protonated carbon dioxide tagged with up to 14 helium atoms, He_N-$HOCO^+$. The first atom preferentially binds to the proton and results in a substantial red-shift of 44 cm^{-1} for the OH stretching vibration, whilst the stepwise attachment of additional atoms up to N = 7 causes small and progressive blue-shifts, which are attributed to the gradual formation of a ring of helium around the carbon atom. The methodology described herein offers a new route to obtain IR spectra of He-tagged ions and provides an insight into ion-solvent interactions at the molecular level.

I. INTRODUCTION

The spectroscopic study of neutral molecules and clusters embedded in liquid helium nanodroplets is well established.[1-3] In a typical experiment, the dopant is added by flowing a beam of helium nanodroplets through a region of low pressure gas or vapor. Absorption spectra can then be recorded using a form of action spectroscopy, commonly referred to as depletion spectroscopy, which utilizes mass-selective ion detection.[4] In contrast to the extensive work on neutral species, far fewer spectroscopic studies have been carried out on charged species formed from doped helium nanodroplets. Of these, the majority have focused on ions that reside inside the droplets, which can be created by photoionization of the neutral dopant, as pioneered by the Drabbels group,[5-7] or alternatively by external production of ions followed by pickup by the droplets, as demonstrated by von Helden and co-workers.[8-11]

Recently, Scheier and co-workers used electron ionization of doped helium nanodroplets to generate He-tagged C_{60}^+ cations, which were subsequently probed using electronic spectroscopy.[12-14] In the electron ionization process, the released energy strips helium from the cation but some molecular ions emerge with helium atoms still attached. Photodissociation spectra were then measured mass-selectively, enabling the electronic spectrum of the ion to be recorded as a function of the number of helium atom tags. Since the ions must be cold in order to retain the weakly-bound tags, the result is a form of cold ion electronic predissociation spectroscopy.

In a recent study, we demonstrated that vibrational predissociation spectra can also be measured for He-tagged cations prepared from helium nanodroplets. In that case, we measured IR spectra for the protonated acetic acid monomer tagged with one and three helium atoms. Our *ab initio* calculations predicted that an attached helium atom will shift the OH stretching vibration by <5 cm^{-1} relative to the bare ion, and ultimately this enabled the identification of two different structural isomers of the molecular ion.[15] Surprisingly, these were the first IR spectra to be measured for either conformer. The success of that study can be attributed to the

rapid cooling of neutral dopants to an equilibrium temperature of 0.37 K inside the nanodroplets, which led to the trapping of metastable dimer structures and, following electron ionization, this generated cold samples of the two ionic conformers tagged with helium.

There are several alternative and well-established methods that can be used to prepare ions tagged with a messenger species, the most common of which are supersonic plasma expansions and cold ion traps. These techniques are well-suited for preparing ions tagged with rare gas atoms or diatomics such as Ne, Ar and H_2, but tagging with helium atoms is significantly more challenging because of the lower temperatures required to attach this weakly interacting species. Nevertheless, several groups have been successful in this endeavor and have reported IR spectra for He-tagged ions.[16-22] Of particular interest are test cases demonstrating that, unlike other tags, helium is a relatively innocent bystander that typically does not change the structure of the ion or the IR spectrum in any substantive way.[18,23,24] As such, helium is considered the ideal messenger species but the established techniques are limited to the attachment of only a few helium atoms.[24,25] In contrast, electron ionization of doped helium nanodroplets can be used to prepare ions tagged with between one and 100 helium atoms, or even more, which allows for a bottom-up approach to studying helium solvation effects.[12-14]

Protonated carbon dioxide, $HOCO^+$, is an interesting example of a He-tagged ion because it exhibits a substantial red-shift in the OH stretching fundamental from 3375.4 to 3328.3 cm^{-1} upon attachment of one helium atom.[26,27] This arises because, just like helium, CO_2 has a low proton affinity and therefore the two species compete for the same proton. As a result, the attached helium atom subtly alters the OH bond and hence its vibrational frequency. Because of this sensitivity to the local helium environment, $HOCO^+$ is a good candidate for probing more extensive helium solvation effects using IR spectroscopy, and this can be achieved by measuring the vibrational frequency shift as a function of the number of attached helium atoms. A similar protocol has previously been used to study helium solvation of small

neutral molecules, such as OCS, CO_2 and N_2O.[28-31] However, an advantage of using ions is that the vibrational frequency shifts will typically be larger and more easily discerned because of the stronger electrostatic interactions with the tag.

In this work, we demonstrate that IR spectra of ions tagged with multiple helium atoms can be obtained using electron ionization of doped helium nanodroplets combined with vibrational predissociation spectroscopy. We describe the methodology used and illustrate the technique for $HOCO^+$ tagged with up to 14 helium atoms.

II. METHODS

A. Experimental

The helium nanodroplet apparatus has been described previously.[32-34] A mean droplet size of ~5000 helium atoms was achieved using a nozzle temperature of 16 K and a helium pressure of 32 bar. The nanodroplet beam was skimmed and passed through a pickup cell to add the dopant. In this case, acetic acid was used as the neutral precursor and a partial pressure of 6×10^{-6} mbar attained an average pickup of one dopant molecule per nanodroplet. After travelling along a 60 cm flight path, the nanodroplet beam entered a quadrupole mass spectrometer (Extrel, MAX-1000) with an electron ionization source operating at an energy of 90 eV. The ionization process generated a range of ions, including $HOCO^+$, both with and without helium atoms attached.

Spectra were recorded by directing the IR beam from a pulsed OPO/OPA laser (LaserVision, Belleview, WA) through the vacuum chamber in a counter-propagating direction relative to the helium nanodroplet beam. The laser beam path was chosen to provide optimal alignment with those droplets located between the electron filament and the center of the deflector that feeds ions into the quadrupole filter of the mass spectrometer, i.e. a short region of roughly 3 cm in length. We note that this alignment is different from that typically used to measure IR spectra for neutral dopants, for which the optimum configuration has the IR beam

fully aligned along the entire helium droplet beam path. The OPO/OPA, which is pumped by an unseeded pulsed Nd:YAG laser (Continuum Surelite II-10), has a pulse energy of ~10 mJ and a linewidth of ~4 cm^{-1}. The wavelength was calibrated using a MIR polystyrene reference film (PerkinElmer). Time-dependent measurements of the mass-selected ion signal enabled discrimination of those ions arriving between 100 and 300 μs after the firing of the Nd:YAG laser. The resulting signal was accumulated by pulse counting electronics and fed to a PC for subsequent data processing. This, in combination with computer-controlled scanning of the output wavelength of the OPO/OPA, was used to record IR spectra of He-tagged $HOCO^+$.

B. Computational details

Ab initio calculations were performed at the MP2/aug-cc-pVTZ level of theory for He_N-$HOCO^+$ for N = 0 to 7 using Gaussian 16 software.[35] Possible binding sites for the first helium atom were identified using a geometry search procedure in which 26 initial geometries were generated by placing the helium atom at selected locations on the surface of a 8 × 8 × 8 Å cube centered on the cation. These locations are the 8 vertices, the 6 face centers and the midpoints of the 12 edges of the cube. The identified structures were then re-optimized using a 'verytight' convergence criterion. Harmonic vibrational frequency calculations were used to test whether the structures corresponded to true energy minima, after which corrections for the zero point energy (ZPE) and basis-set superposition error (BSSE) were made. Subsequently, for each of the three lowest energy structures for N = 1, an additional helium atom was placed at 26 different locations on the surface of a 8 × 8 × 8 Å cube, which generated a total of 78 initial geometries for the N = 2 search procedure. Each optimized structure was tested as described above, and the procedure was repeated for all values of N up to N = 7.

The harmonic vibrational frequencies for the OH stretch were empirically scaled by a factor of 0.9556 to allow comparison with the experimental spectra. This value is derived by scaling the computed value for untagged $HOCO^+$ so that it equals the known experimental

value of 3375.4 cm^{-1}.[26] Anharmonic vibrational frequency calculations were also performed for N = 1 to 4 by using generalized second-order vibrational perturbation theory (GVPT2).

III. RESULTS AND DISCUSSION

A. Mass spectrometry

A mass spectrum is presented in Fig. 1, which was obtained using electron ionization of helium nanodroplets doped with an average of one acetic acid molecule per droplet. The statistical nature of the pickup process means that some droplets will contain more than one molecule while others contain no dopant. The spectrum represents the difference in ion signal measured with and without the dopant, thus removing the strong He_N^+ peaks that are normally observed at *m*/*z* 4, 8, 12, etc. The remaining signal therefore originates from ionization of neutral acetic acid molecules and their clusters embedded inside the helium nanodroplets. The most intense peaks correspond to cation fragments CH_3CO^+ (*m*/*z* 43) and $(CH_3COOH)H^+$ (*m*/*z* 61), which are primarily formed by dissociative ionization of metastable neutral acetic acid dimers, whilst the $HOCO^+$ peak at *m*/*z* 45 principally derives from the neutral *trans*-monomer.[36]

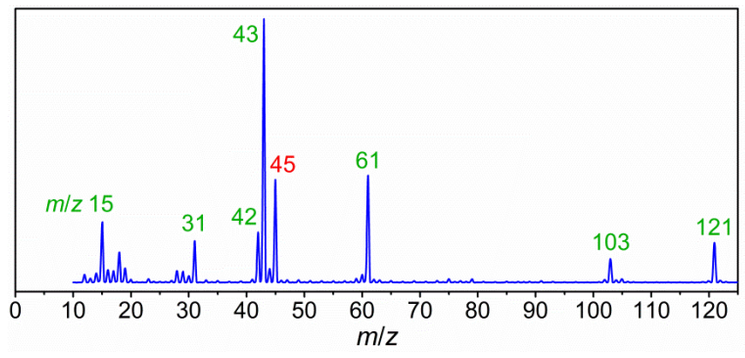

FIG. 1. Mass spectrum derived from electron ionization of helium droplets doped with acetic acid under conditions where the average number of dopant molecules per droplet is close to one. The electron energy was 90 eV and the background signal from undoped droplets has been subtracted so that the molecular ion peaks are clearly observed. The mass-to-charge ratios of the most abundant ions are indicated and the $HOCO^+$ channel is highlighted in red.

B. IR spectroscopy by detecting bare $HOCO^+$

The IR depletion spectra shown in Fig. 2 were measured by detecting wavelength-dependent changes in the mass-selected ion signal at *m*/*z* 45 ($HOCO^+$) under a variety of experimental conditions. A decrease in nozzle temperature from 16 K to 12 K leads to an increase in droplet size, whilst a reduction in the data acquisition gate delay from 600 μs to 100 μs favors the detection of species located close to the mass spectrometer when the laser pulse is triggered, which is the region where ions are produced. Both of these criteria have a considerable influence on the relative intensities of the IR peaks at 3337 and 3585 cm^{-1}.

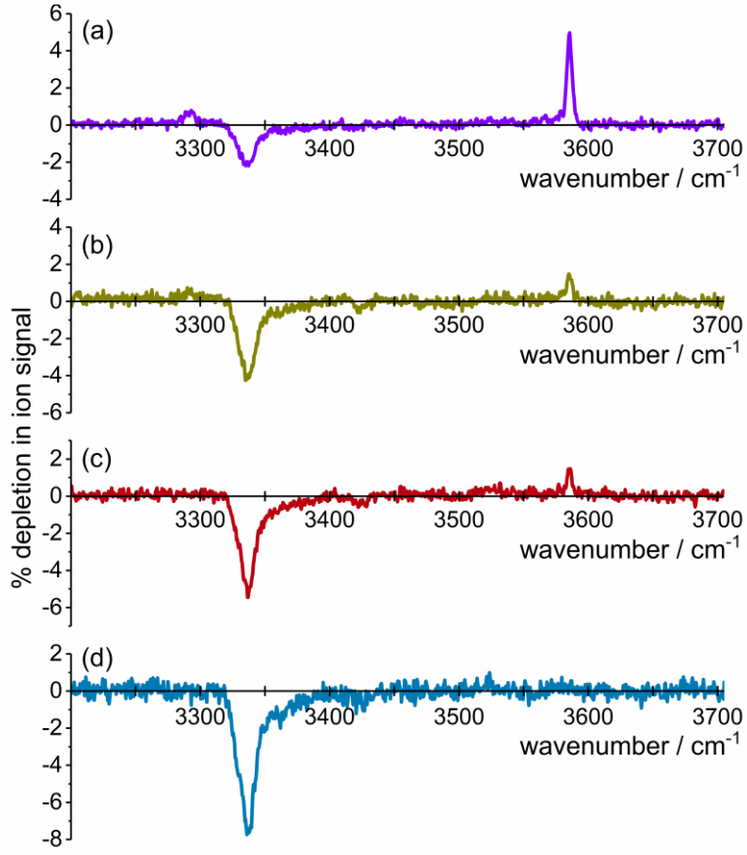

FIG. 2. IR depletion spectra recorded at *m*/*z* 45 under a variety of experimental conditions. The nozzle temperature and data acquisition gate delay time are (a) 16 K and 600 μs, (b) 12 K and 600 μs, (c) 16 K and 100 μs, (d) 12 K and 100 μs.

In Fig. 2(a), the strong positive-going peak at 3585 cm^{-1} is assigned to the OH stretching mode of the neutral acetic acid monomer. The other positive-going peak at 3292 cm^{-1}, which is weak, corresponds to the stretching mode of a hydrogen-bonded OH group in a metastable neutral acetic acid dimer.[36] A slightly broader peak is observed at 3337 cm^{-1} that exhibits a negative depletion owing to an enhancement in ion signal at *m*/*z* 45. This clearly differentiates it from the positive-going peaks assigned to IR absorption by neutral dopants and we tentatively assign it to the OH stretching mode in $HOCO^+$. The known frequency of this vibration for the bare ion is 3375.4 cm^{-1},[26] whilst the value for He-$HOCO^+$ is 3328 cm^{-1}.[27] This suggests that the experimental peak observed at 3337 cm^{-1} arises from IR absorption by $HOCO^+$ tagged with one or more helium atoms originating from the nanodroplet and that these helium atoms redshift the OH stretching frequency (see later).

To further investigate the origin of the negative-going peak at 3337 cm^{-1}, it is desirable to measure IR spectra at the parent mass channels corresponding to He_N-$HOCO^+$. The mass spectrum in Fig. 1 shows little evidence of ion signal originating from He-tagged $HOCO^+$ but a vertically expanded view in Fig. 3 allows us to identify such peaks for $HOCO^+$ complexed with between 1 and 14 helium atoms. These peaks, seen at *m*/*z* 49, 53, 57, etc., have intensities approximately two orders of magnitude lower than for the bare $HOCO^+$ ion at *m*/*z* 45. Despite the low ion yields, it has been possible to measure their IR spectra by scanning the IR wavelength while monitoring the ion signal intensity.

In Fig. 3, labels are also shown for those mass peaks that can contain ion signal from He-tagged protonated acetic acid, He_M-$(CH_3COOH)H^+$. These peaks lie at *m*/*z* 65, 69, 73, etc, which are at the same position as He_N-$HOCO^+$ for $N \geq 5$. Due to the limited resolution of our mass spectrometer, we are unable to resolve these two distinct species in the mass spectrum. However, we showed in a previous publication that He-tagged protonated acetic acid and $HOCO^+$ have very different IR spectra in the OH stretching region,[15] enabling the two ions to be readily distinguished (see Fig. S1).

The Journal of Chemical Physics

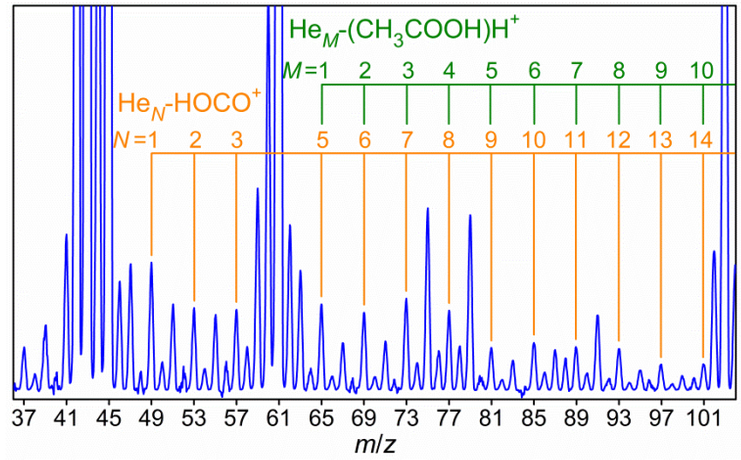

FIG. 3. Expanded view of part of the mass spectrum shown in Fig. 1, enabling the low intensity peaks to be discerned. Two series of ions are labelled, corresponding to He-tagged $HOCO^+$ and He-tagged protonated acetic acid.

C. IR spectroscopy of He_N-$HOCO^+$ for $N \leq 3$

In Fig. 4, IR spectra for He_N-$HOCO^+$, where N = 1, 2 and 3, are compared with an IR spectrum recorded at the mass of the bare ion (N = 0). The spectra for the He-tagged ions are dominated by a positive-going depletion peak at ~3330 cm^{-1}, which lies close to the negative-going peak at 3337 cm^{-1} in the bare ion spectrum. These near isoenergetic features of opposing polarity indicate that IR absorption results in detachment of helium atoms from the tagged ions, in accordance with the photodissociation process:

$$h\nu + He_N\text{-}HOCO^+ \rightarrow (He_N\text{-}HOCO^+)^* \rightarrow N\,He + HOCO^+$$

Thus our experimental technique is a type of helium messenger vibrational predissociation spectroscopy. We deduce that the enhancement in the bare ion signal [see Fig. 4(a)] originates from the complete stripping of all helium atoms from He_N-$HOCO^+$ for a wide range of N values, as a result of IR absorption and in accordance with the photodissociation process shown above.

This arises because the total binding energy of all of the helium atoms is lower than the photon energy, as shown by the *ab initio* calculations discussed in Section III E. In comparison, the depletion in He_N-$HOCO^+$ signal for each selected value of N represents IR absorption by that species only.

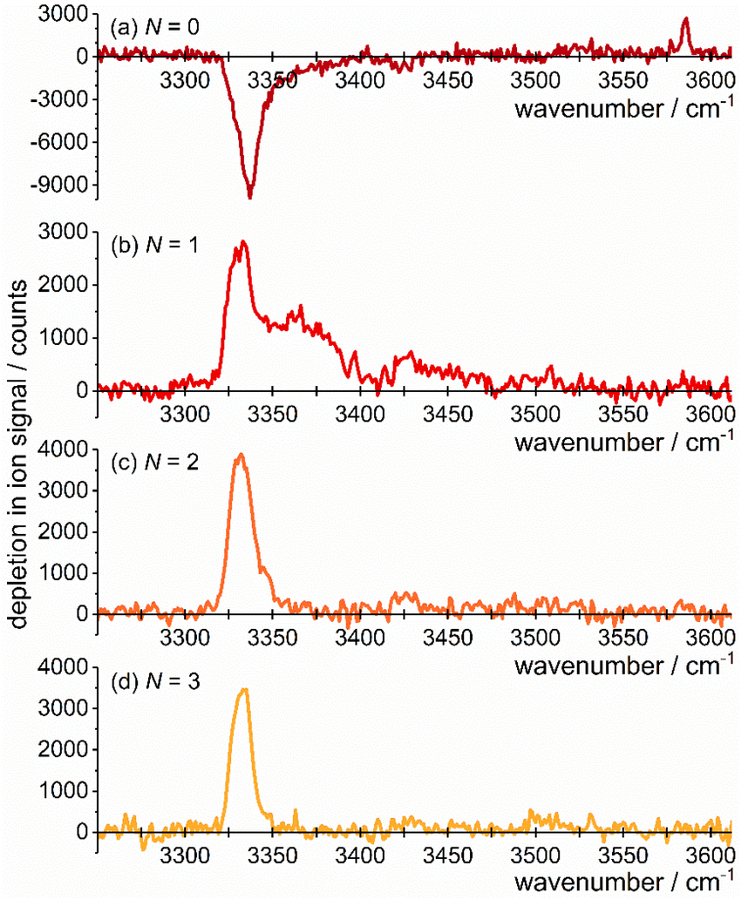

FIG. 4. IR depletion spectra measured at (a) *m*/*z* 45, (b) *m*/*z* 49, (c) *m*/*z* 53, and (d) *m*/*z* 57, where these mass channels correspond to ion fragments He_N-$HOCO^+$ with N = 0, 1, 2 and 3, respectively.

The dominant feature observed at ~3330 cm^{-1} in Fig. 4(b) is assigned to the OH stretching mode in He-$HOCO^+$, i.e., N = 1. This is confirmed by a comparison with the experimental and calculated values of 3328.3 and 3317.8 cm^{-1} obtained by Dopfer *et al.*[27] Simulations of the rotational profile have been performed using PGOPHER software[37,38] and

compared with the experimental band shape (see Fig. S2(a), Table S1). The agreement is rather poor, which suggests a non-equilibrium thermal distribution. This is not surprising given that ion cooling in helium nanodroplets is known to be highly nonthermal.[39,40] Nevertheless, a 'temperature' of between 20 and 60 K does reproduce some of the observed band broadening. It is also possible that other processes contribute significantly to the broadening, such as large amplitude motion at the zero-point energy, particularly for the intermolecular bending and stretching vibrations. Further insight could be obtained by modelling this effect using path integral molecular dynamics simulations.

The red-shift of the band center relative to the value of 3375.4 cm^{-1} for the bare ion indicates that a proton-bound helium atom significantly perturbs the OH stretching motion of the $HOCO^+$ cation. In contrast, the vibrational frequencies of the $N = 2$ and 3 spectral features in Figs. 4(c) and 4(d) are very close to the $N = 1$ band, indicating that the attaching of a second and third helium atom has a far weaker effect on the OH stretching motion of $HOCO^+$.

An unusual feature in the $N = 1$ spectrum [see Fig. 4(b)] is a secondary absorption extending from ~3340 to ~3400 cm^{-1}, which is absent from the $N = 2$ and 3 spectra. This broad feature must therefore arise only from the binding of a single helium atom to $HOCO^+$. Interestingly, the earlier work on He-$HOCO^+$ by Dopfer *et al.*, which utilized a pulsed supersonic expansion ion source, obtained a somewhat different spectral profile in the region immediately to the blue of the main feature at 3328 cm^{-1}.[27] A tail extending to ~3358 cm^{-1} was observed and attributed, at least in part, to rotational band structure arising from a contraction of the intermolecular bond upon excitation of the OH stretch fundamental. A weak peak at ~3364 cm^{-1} was also observed but not assigned. Even though there is some evidence of these features in the present work, they are somewhat dwarfed by the aforementioned broad band centered at ~3370 cm^{-1}.

The difference between our spectral profile and that of Dopfer *et al.*[27] might arise from the different methods used for generating the tagged ions. In gas-phase experiments that use a

supersonic expansion, the neutral precursor is directly ionized via electron impact, whilst ion cooling occurs via inelastic collisions with the buffer gas. In contrast, electron ionization of doped helium nanodroplets involves ionization of a helium atom near the surface of the droplet, followed by resonant charge migration between helium atoms and, finally, charge transfer to the cold dopant molecule. This leads to the generation of a hot ion and subsequent cooling is achieved by evaporation of helium atoms. The messenger tagged ions generated by the two distinct techniques may differ in terms of the rotational and vibrational state populations, as well as in the relative abundance of various isomers. Therefore, there is a possibility that metastable $N = 1$ structures are generated and survive using the helium nanodroplet technique. A similar observation is well documented for neutral clusters embedded in helium nanodroplets.[36,41-43]

To further explore the source of the broad feature at ~3370 cm^{-1}, we have performed *ab initio* calculations at the MP2/aug-cc-pVTZ level of theory for $HOCO^+$, both with and without an attached helium atom. A geometry search procedure was used to find prospective stable structures for $He\text{-}HOCO^+$ and this led to the identification of three possible locations for the helium atom, as illustrated in Fig. 5, where the lowest energy structure (1A) is the proton-bound conformer previously identified by Dopfer *et al.*[27] The BSSE- and ZPE-corrected relative energies for the three calculated structures are 0.0, 1.28 and 1.88 kJ mol^{-1}, respectively, whilst scaled harmonic vibrational frequency calculations predict values of 3320, 3377 and 3376 cm^{-1} for the OH stretching fundamental (see Table S2). Comparison with the experimental spectrum shown in Fig. 4(b) therefore confirms that the most intense feature centered at ~3330 cm^{-1} derives from structure 1A, in which the helium atom is proton-bound, whilst the broad feature at ~3370 cm^{-1}, most likely derives from structures 1B and 1C.

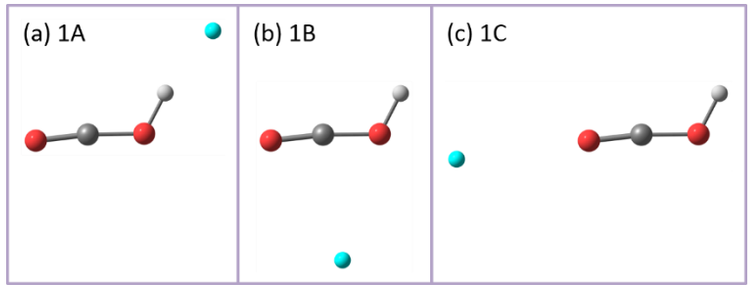

FIG. 5. Optimized structures for He-$HOCO^+$ calculated using the MP2/aug-cc-pVTZ level of theory. The blue circle represents the helium atom. These structures have BSSE and ZPE corrected relative energies of (a) 0.0 kJ mol^{-1}, (b) 1.28 kJ mol^{-1} and 1.88 kJ mol^{-1}.

We have also considered whether alternative cationic species that have an *m*/*z* of 49 might contribute to the broad IR bands including various isomers of (a) He-tagged protonated acetaldehyde and He-tagged protonated ethylene oxide (He-$C_2OH_5^+$), (b) protonated methanediol and protonated methyl peroxide ($CO_2H_5^+$) and (c) protonated ozone (O_3H^+). The structures and calculated IR spectra are presented in the Supplementary Material in Figs. S4 and S5. However, these ions can be discarded from consideration either because of poor agreement between calculated and experimental IR spectra or because they are unlikely to fragment following single photon absorption. In contrast, structures 1B and 1C fulfil both of these criteria.

Rotational contour simulations[37,38] performed at a temperature of 40 K for He-$HOCO^+$ structures 1B and 1C [see Fig. S2(b) and Table S1 in the Supplementary Material] are able to account for the spectral region between ~3360 to ~3380 cm^{-1}, as well as the spectral feature centered at 3397 cm^{-1}, whereby the latter is a close match to a rotational sideband in structure 1C. For the spectral region between 3340 and 3360 cm^{-1}, a possible assignment is to vibrational hot bands associated with structure 1A. Our anharmonic calculations predict that these will occur at 3343 and 3355 cm^{-1} [see Table S3 and Sec. I(ii) in the Supplementary Material]. However, the bands might be broadened due to the large amplitude motion of the thermally populated intermolecular bending vibration. We therefore propose that several different factors

contribute to the broad feature, including metastable isomers and vibrational hot bands. This conclusion is similar to that proposed by Bieske and co-workers to explain comparable broad features in Ar_N-HCO^+, particularly for N = 3.[44] Delocalization of the helium atom and large amplitude motion at the zero-point energy for metastable structures 1B and 1C may also contribute to the band broadening.

In Fig. 4, a relatively weak feature is observed at ~3426 cm^{-1} in the spectra measured for N = 1 and 2, and which is just about discernible above the noise for N = 3. This feature is blue-shifted by ~96 cm^{-1} relative to the OH stretching fundamental and has previously been observed for N = 1 by Dopfer *et al.*[27] who tentatively assigned it to the $\nu_1 + \nu_s$ combination band, where ν_1 is the OH stretching mode and ν_s is the low frequency He-H^+ intermolecular stretching mode. A comparable combination band was observed in the spectrum of Ar-tagged $HOCO^+$,[27,45] but was barely perceptible for Ne-tagged $HOCO^+$.[27] Harmonic calculations for the Ar- and Ne-tagged ions strongly supported the assignments to $\nu_1 + \nu_s$; however equivalent calculations for He-tagged $HOCO^+$ showed poor agreement with experiment. As a result, Dopfer *et al.*[27] stated that an alternative assignment to an intramolecular combination band, such as $\nu_2 + \nu_3$ or $\nu_2 + \nu_4$, could not be ruled out. In this notation ν_2 is the O-C-O antisymmetric stretch, ν_3 is the O-C-O symmetric stretch and ν_4 is the C-O-H in-plane bending mode. To investigate this assignment further, we have performed anharmonic vibrational frequency calculations for the global minimum energy structures for He_N-$HOCO^+$, where N = 0 to 3. Selected results are presented in Table I.

TABLE I. Selected results from anharmonic vibrational frequency calculations for the global minimum structures of He_N-$HOCO^+$ where N = 0 to 3.

N	ν_1		$\nu_1 + \nu_s$		$\nu_2 + \nu_3$		$\nu_2 + \nu_4$	
	ν / cm^{-1}	I [a]	ν / cm^{-1}	I [a]	ν / cm^{-1}	I [a]	ν / cm^{-1}	I [a]
0	3351	622	-	-	3589	7.3	3388	9.6
1	3306	755	3442	0.5	3600	7.6	3398	24.6

2	3305	741	3445	0.3	3599	7.5	3398	24.7
3	3306	721	3441	0.3	3599	7.2	3402	23.4

[a] IR intensity in km mol^{-1}

The calculated IR intensities for the $\nu_1 + \nu_s$ combination band are at least three orders of magnitude smaller than for the ν_1 fundamental band, making the assignment of this transition to the 3426 cm^{-1} band seem unlikely. Calculated intensities for the $\nu_2 + \nu_3$ combination band are significantly higher but the calculated frequencies are >160 cm^{-1} to the blue of the experimental band at 3426 cm^{-1}. Instead, the anharmonic calculations indicate that the most likely assignment is to the $\nu_2 + \nu_4$ combination band, which has an even higher predicted intensity and a frequency lying within 40 cm^{-1} of the experimental value. We further note that the calculated frequency for the ν_1 fundamental in $HOCO^+$ (N = 0) is 24 cm^{-1} lower than the known experimental value of 3375.4 cm^{-1}, indicating that the anharmonic calculations tend to underestimate the frequencies. If this is accounted for by blue-shifting the $\nu_2 + \nu_4$ band frequency by 24 cm^{-1} for N = 1 to 3 then the difference between experiment and calculations is reduced to ≤4 cm^{-1}, providing additional support for this assignment.

As mentioned earlier, the $\nu_1 + \nu_s$ combination band was previously observed in experimental IR spectra for Ar- and Ne-tagged $HOCO^+$ and it was presumed that the equivalent band should also be observed for He-$HOCO^+$. To address this point we have performed anharmonic calculations for Ar- and Ne-tagged $HOCO^+$ and we have determined IR intensities of 313 and 15 km mol^{-1}, respectively, for the $\nu_1 + \nu_s$ band (see Table S4). These intensities are several orders of magnitude larger than predicted for the He-tagged ion (0.5 km mol^{-1}), thus discounting the above presumption. However, we note that the GVPT2 method is better suited to small, rigid molecules than weakly bound complexes, and so the calculated structure deriving from intermolecular vibrations should be treated with some caution. Thus, while we favor an assignment to the $\nu_2 + \nu_4$ combination band, the $\nu_1 + \nu_s$ transition cannot be completely ruled out.

D. IR spectroscopy of He_N-$HOCO^+$ for $5 \leq N \leq 14$

In Fig. 6, we present IR spectra measured in the region of the OH stretching fundamental in He_N-$HOCO^+$ for selected values of N from 1 to 14. No spectrum is shown for N = 4 because the ion yield from He_4-$HOCO^+$ is likely to be two orders of magnitude lower than the ion yield from untagged protonated acetic acid, $(CH_3COOH)H^+$, which has the same m/z. The figure illustrates the N-dependent blue-shift in the peak center from 3331 cm^{-1} at N = 1 to 3340 cm^{-1} at N = 14. This indicates a stiffening of the OH bond upon the attachment of additional helium atoms.

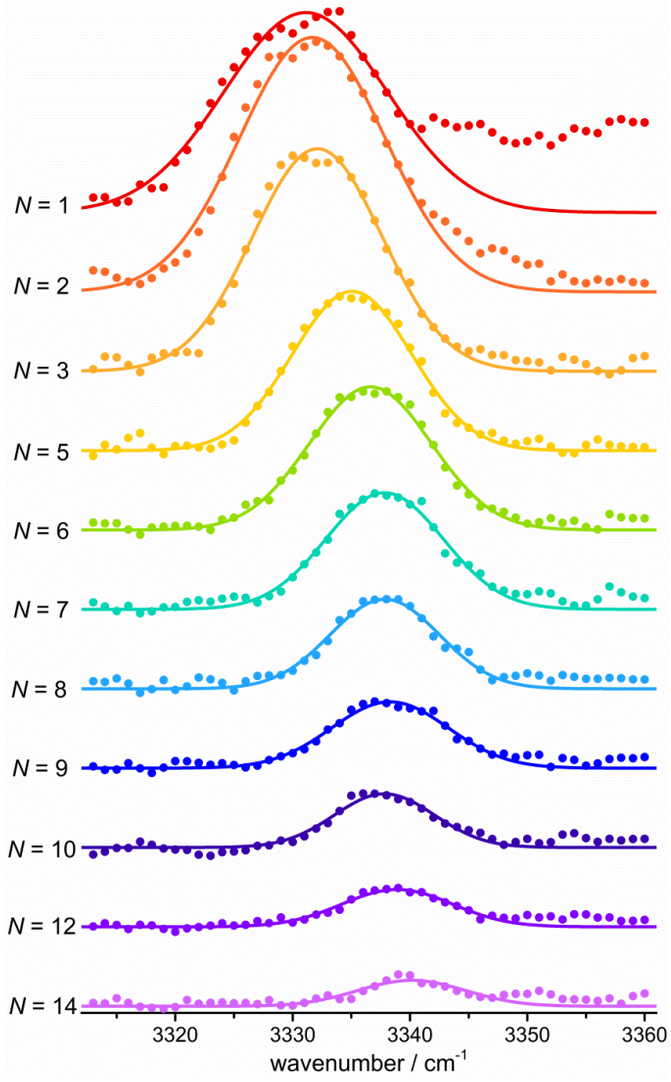

FIG. 6. IR depletion spectra measured for the OH stretching mode at mass channels corresponding to He_N-$HOCO^+$. The filled circles denote experimental data points and the solid lines represent fits to a single Gaussian function.

To gain further insight into the band shift with increasing *N*, we have extended our *ab initio* calculations for He_N-$HOCO^+$ up to a value of $N = 7$. The local minima structures identified in this work are shown in Figs. S6 to S11, whilst calculated energies and vibrational frequencies are given in Tables S5 to S10. We note that such calculations will be indicative rather than exact because the weakly-bound complexes are likely to be very floppy owing to relatively flat potential energy surfaces, which means that nuclear quantum dynamics will be important for the helium atoms.

We have found that the number of local energy minima identified using our geometry search procedure increases dramatically from 9 at $N = 4$ to a total of 18 at $N = 5$, 6 and 7. Many of these structural isomers are near-isoenergetic and, as such, any helium atoms in locations with similar binding energies are likely to be delocalized.[46,47] This result confirms our assertion that it is not entirely realistic to assign a particular isomeric structure to the IR spectrum measured for each value of *N*, particularly for higher *N*. However it is still a useful exercise to calculate the trend in OH stretch frequencies as a function of *N* and to compare this trend with the experimental results. The most straightforward way to achieve this is by first considering the calculated global minimum structures.

The minimum energy structure for $N = 1$ was shown in Fig. 5(a), whilst those for $N = 2$ to 7 are presented in Fig. 7. For $N = 1$, the helium atom is located at a distance of just 1.69 Å from the proton but far from the oxygen and carbon atoms. The addition of a second helium through to the sixth helium atom leads to the stepwise formation of a five-membered ring around the carbon atom, whilst the first helium atom remains in an almost fixed location at ~1.71 Å from the proton. The distance between the carbon atom and helium ring atoms is ~2.8 Å and the ring lies in a plane roughly perpendicular to the O-C-O axis. The formation of a ring of helium atoms is reminiscent of previous IR spectroscopy studies of small neutral molecules solvated by helium, such as OCS, CO_2 and N_2O.[28-31]

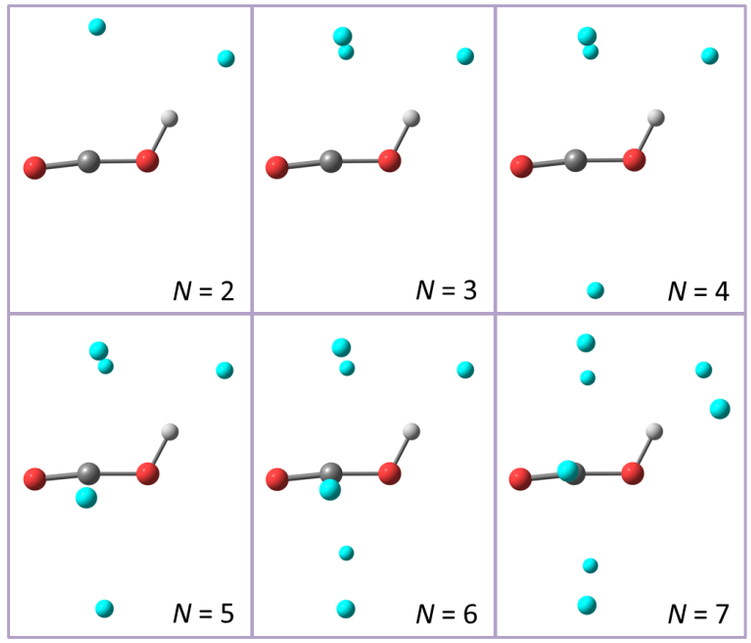

FIG. 7. Global minimum energy structures for He_N-$HOCO^+$ for N = 2 to 7, calculated using the MP2/aug-cc-pVTZ level of theory.

The seventh helium atom preferentially binds to the proton end of the ion, causing the helium atom closest to the proton to shift slightly, which results in an increased $He\text{-}H^+$ separation of 1.73 Å. As such, the seventh helium atom appears to play a role in connecting the first added helium atom with the ring atoms, perhaps beginning the process of forming a complete solvation shell around the cation.

Figures 8(a) and 8(b) show alternative views for the two lowest energy structures calculated for N = 6, illustrating that the helium atoms in the five-membered ring are not equally spaced. The largest separation between two adjacent helium atoms in the ring is 4.39 Å, whilst the smallest separation of 2.82 Å is between the ring atoms closest to the proton. Separations between other adjacent helium ring atoms are ~3.0 Å. Figs. 8(c) and 8(d) show the global minimum structures for N = 7 calculated with and without a ZPE correction, respectively. The latter contains a six-membered ring of helium atoms centered on the carbon atom, where the separations between adjacent helium atoms vary only slightly from 2.74 to 2.85 Å. The ZPE

corrected energy of this structure is 0.40 kJ mol^{-1} higher than for the five-membered ring conformer shown in Fig. 8(c). This is attributed to the stiffness of the 6-member ring, which results in higher vibrational frequencies for various intermolecular modes and the OH torsional mode.

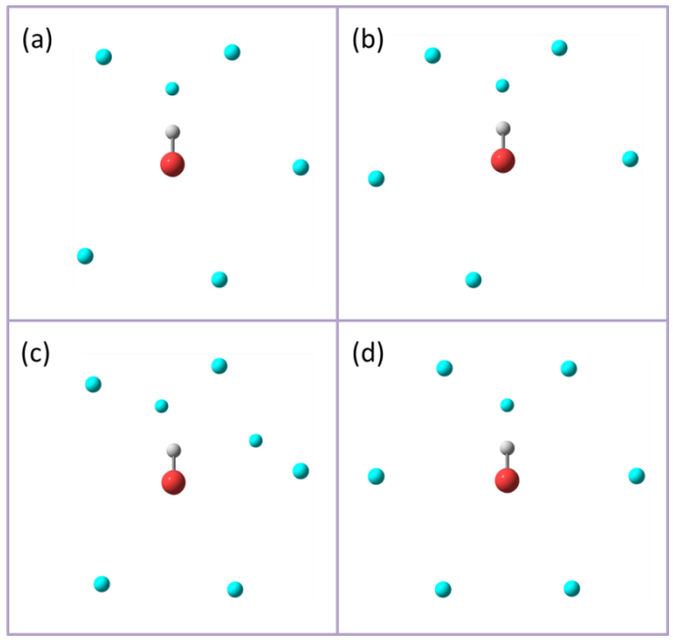

FIG. 8. Calculated structures for He$_N$-HOCO$^+$ for (a) the lowest and (b) second lowest energy conformers for N = 6. Also shown are the lowest energy conformers for N = 7 when the ZPE correction is (c) included and (d) not included. These structures are viewed from the terminal O-atom end of the cation.

E. *N*-dependent shift in OH stretching frequency

Figure 9 shows the frequency shifts in the OH stretching vibration that result from attaching N helium atoms to HOCO$^+$. The experimental values correspond to the difference between the centers of the fitted Gaussian functions shown in Fig. 6 and the known experimental value for the bare ion of 3375.4 cm^{-1}.[26] Calculated values from scaled harmonic frequencies are presented for the global minimum energy structures up to N = 7, whilst unscaled anharmonic frequency shifts are available up to N = 4 only. In Fig. 9(a), there is good agreement between

the experimental and anharmonic frequency shifts for N = 1, 2 and 3 (there is no experimental value for N = 4, as explained earlier). This illustrates that the substantial red-shift in OH stretching frequency of 44 cm^{-1} from N = 0 to 1 is well described by the anharmonic calculations, whereas the harmonic calculations slightly overestimate the strength of the intermolecular interaction, resulting in a red-shift of 11 cm^{-1} from the experimental value. This confirms that anharmonicity plays a significant role in the motion of the proton between the CO_2 entity and the attached helium atom.

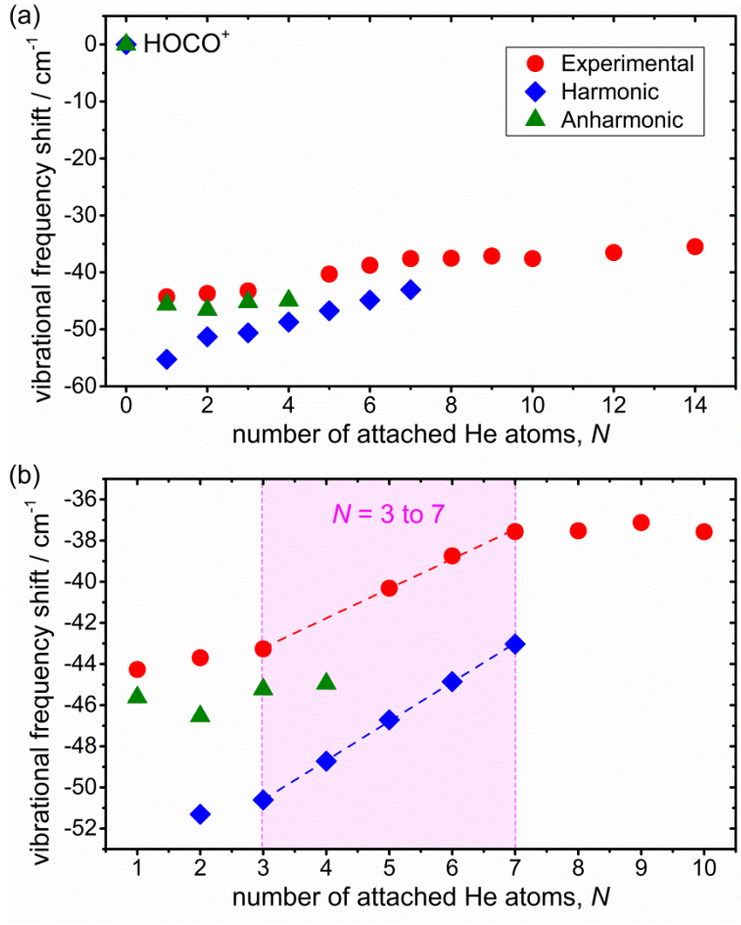

FIG. 9. Experimental frequency shift in the OH stretching vibration for He_N-$HOCO^+$ is plotted against N and compared with values from scaled harmonic (x0.9556) and unscaled anharmonic vibrational frequency calculations. (b) is an expanded view of part of the plot shown in (a).

In Fig. 9(b), an expanded view shows the subtle shifts in the experimental OH stretching frequency observed for $1 \leq N \leq 10$. In this region, the largest shifts occur between $N = 3$ and 7. A linear fit to the experimental data within this range indicates a blue-shift of 1.44 cm^{-1} for each added helium atom, compared with a predicted blue-shift of 1.90 cm^{-1} per atom from the scaled harmonic frequency calculations. However, it is important to note that the calculated results presented in Fig. 9 are for the global minimum structures only. Therefore, in a rudimentary attempt to take into account the delocalization of the helium atoms, we have considered a range of local energy minima structures that give alternative locations of the helium atoms relative to the ion. By considering the average value of the OH stretching frequencies for conformers with energies < 0.5 kJ mol^{-1} above the global minimum structure for each value of N (see Tables S2 and S5 to S10), we have calculated a blue-shift of 1.56 cm^{-1} per helium atom, in closer agreement with the experimental results.

In Table II, we present further results for the global minimum structure at each value of N. An approximately linear relationship is observed between the OH bond length and OH stretching frequency but with a negative correlation, as expected. The OH bond length increases by 0.0026 Å upon addition of the first helium atom, which is accompanied by a decrease in the central CO bond length by 0.0019 Å and a small increase in the terminal CO bond length of 0.0004 Å (see Table S11 and Fig. S12). Upon attachment of further helium atoms, a decrease in all intramolecular bond lengths and the COH angle is generally observed, along with an increase in the OCO angle. These structural changes in the ion core directly report on the ion-solvent interactions. Furthermore, our calculations indicate that the OH stretching vibration shows a larger N-dependent frequency shift than any other intramolecular fundamental mode (see Table S12 and Fig. S13) and therefore it is a more sensitive probe of helium solvation.

TABLE II. *N*-dependence of the OH stretching frequency, equilibrium OH bond length and binding energy of the *N*th helium atom for He_N-$HOCO^+$.

N	Experimental	Anharmonic	Harmonic frequency calculations		
	ν / cm^{-1}	ν / cm^{-1}	ν / cm^{-1}	r_{OH} / Å	D_0 / cm^{-1}
0	-	3351.3	3375.4	0.9879	-
1	3331.1	3305.7	3320.1	0.9905	154
2	3331.7	3304.7	3324.1	0.9904	120
3	3332.1	3306.1	3324.8	0.9903	94
4	-	3306.3	3326.6	0.9902	66
5	3335.1	-	3328.7	0.9901	64
6	3336.6	-	3330.5	0.9900	62
7	3337.8	-	3332.3	0.9900	54
8	3337.9	-	-	-	-

The BSSE and ZPE corrected energy for removing a single helium atom, D_0, decreases from a maximum value of 154 cm^{-1} at $N = 1$ to just 54 cm^{-1} at $N = 7$ (see Table II), and it is anticipated to be even smaller at higher values of N. These low D_0 values support our earlier hypothesis that absorption of an IR photon at ~3330 cm^{-1} will strip all of the helium atoms from the ion for the values of $N \leq 14$ investigated in this work, and most likely up to $N = 70$ or more.

The partial atomic charges in $HOCO^+$ have been calculated for each global minimum structure of He_N-$HOCO^+$, where N = 1 to 7. These values correspond to the electrostatic potential (ESP) derived charges and were determined using the CHELPG scheme.[48] Even though bare $HOCO^+$ is often referred to as protonated CO_2, our calculations show that the partial charge on the carbon atom is approximately double that on the hydrogen atom. Furthermore, there is a strong correlation between the location of the positive partial charges and the preferred solvent binding sites, i.e., at the hydrogen and carbon atoms. This confirms that the dominant ion-solvent interactions are electrostatic in nature.

The partial charges show small but clear trends with N (see Table S13 and Fig. S14). Attachment of the first helium atom leads to a decrease in the positive charge on the hydrogen

atom from 0.49*e* to 0.40*e* and an induced charge of 0.06*e* on the helium atom. This coincides with a lengthening of the OH bond and a redistribution of partial charge within the ion, including an increased positive charge on the carbon atom. Another notable change occurs when the sixth helium atom is added, resulting in a decrease in partial charge on the carbon atom from 0.83*e* to 0.77*e* and an increase in the total charge on the helium ring atoms from 0.04*e* to 0.07*e*. The significance of the sixth helium atom is that it completes the formation of a 5-membered ring around the carbon atom, providing a partial electrostatic shield between the positive charge on the carbon and any additional helium atoms that may subsequently be added. Thus, the partial charge calculations shed light on the electrostatic ion-solvent interactions and the resulting structural changes in the ionic core. Furthermore, even though the total charge on He_N-$HOCO^+$ remains constant for all values of N, the magnitude of the partial charge on each atom in $HOCO^+$ is lower for $N = 6$ and 7 than for the unsolvated ion ($N = 0$). This suggests that any additional helium atoms beyond $N = 6$ will be less perturbed by the ionic impurity and has implications for the onset of superfluidity once a critical value of N is reached.

Finally we note that, despite our reservations, static *ab initio* calculations have been successful in modelling the spectroscopic behavior of He_N-$HOCO^+$ up to a value of $N = 7$ and have shown good agreement with experiment. However, this study and future experimental studies on the solvation of ions in helium would benefit from quantum molecular dynamics simulations.

F. Remarks on the experimental technique

The apparatus can be used to measure IR spectra for both neutral molecules and He-tagged ions. It is a relatively simple task to switch between the two modes of operation and this is primarily achieved by changing the gate time settings on the data acquisition electronics. This capability allows for a structural comparison of the neutral precursor and the fragment ion, and can provide information on the electron ionization process.[15] Furthermore, the ability to prepare

metastable neutral structures inside helium nanodroplets allows for the creation of new ionic structures that might be difficult or impossible to form using other techniques. However, despite these advantages, there is still scope for improvement. In particular, the present experimental set-up has only one mass-selective stage to record mass-selected IR spectra. In the case of He-tagged ions, an improvement would be to employ tandem mass spectrometry, where the first stage selects a particular ion and the second stage detects a particular photodissociation product. Such an arrangement would deliver a zero background ion signal at off-resonance wavelengths and so would massively improve the signal/noise ratio.

The benefit of mass-selectivity is particularly evident when comparing the present technique with previous IR spectroscopy studies of He-tagged neutral molecules, such as OCS, CO_2 and NO_2.[28-31] Those studies were limited to small molecules because of a lack of mass-selectivity and, as a result, substantial deconvolution of rotationally-resolved IR spectra was required in order to determine the *N*-dependent behavior. Fortunately, because the present technique does not suffer from the same restriction, it can readily be extended to the study of larger molecular ions. Now the limiting factor on the suitability of an ion will likely be whether there is a measurable frequency change in one of the vibrational modes when the number of attached messenger tags is varied. When there is negligible change, the measured spectrum will still be of considerable value because it will be representative of the bare ion. As such, our technique can be used to report on (i) the bare ion,[15] and/or (ii) ion solvation effects.

It is a relatively straightforward task to extend this technique to other weakly-bound messenger tags, such as, neon, argon or molecular hydrogen. This could be achieved by doping the helium nanodroplets with the new tag species prior to electron ionization. Because interactions with alternative tags will be stronger than for helium, the new tag will preferentially bind to the neutral dopant. Following electron ionization, ions tagged with the new species will be generated, which can subsequently be probed using mass-selective IR depletion spectroscopy.

IV. CONCLUSIONS

We have demonstrated that electron ionization of neutral acetic acid embedded in helium nanodroplets can be used to generate a small ion, $HOCO^+$, tagged with up to 14 helium atoms. IR spectra of the mass-selected ions reveal that the OH stretching vibration is a sensitive probe of the gradual solvation of the ion in helium. In particular, the combined experimental and theoretical data indicate that the first helium atom preferentially binds to the proton and, as further helium atoms are added, a ring of helium is formed around the carbon atom. As well as subtly changing the structure of the ion core, the most strongly bound helium atoms alter the distribution of charge. This may have implications for the formation of the first few solvation layers around a dopant ion following its introduction into a helium nanodroplet. Finally, we note that the experimental technique described here provides an alternative to other techniques for recording IR spectra of helium-tagged ions and can in principle be applied to a wide range of ions, both large and small.

SUPPLEMENTARY MATERIAL

See supplementary material for details of rotational contour simulations of the OH stretching band in He-$HOCO^+$; *ab initio* calculations on local minima structures for $HOCO^+$ tagged with up to seven helium atoms, one argon atom and one neon atom; *ab initio* calculations for He-$C_2OH_5^+$, $CO_2H_5^+$ and O_3H^+.

ACKNOWLEDGEMENTS

The authors wish to thank the Leverhulme Trust for providing financial support (grant number RPG-2016-308) for this work. Helpful discussions with Gary E. Douberly are also gratefully acknowledged. The computational work used the SPECTRE High Performance Computing Facility at the University of Leicester.

REFERENCES

1. J. P. Toennies, A. F. Vilesov, *Angew. Chem. Int. Ed.* **43**, 2622 (2004).
2. C. Callegari, W. E. Ernst, Helium Droplets as Nanocryostats for Molecular Spectroscopy - from the Vacuum Ultraviolet to the Microwave Regime. Handbook of High-resolution Spectroscopy, Wiley, 2011.
3. S. Yang, A. M. Ellis, *Chem. Soc. Rev.* **42**, 472 (2013).
4. M. Hartmann, R. Miller, J. P. Toennies, A. F. Vilesov, *Phys. Rev. Lett*. **75**, 1566 (1995).
5. S. Smolarek, N. B. Brauer, W. J. Buma, M. Drabbels, *J. Am. Chem. Soc.* **132**, 14086 (2010).
6. N. B. Brauer, S. Smolarek, X. Zhang, W. J. Buma, M. Drabbels, *J. Phys. Chem. Lett.* **2**, 1563 (2011).
7. X. Zhang, N. B. Brauer, G. Berden, A. M. Rijs, M. Drabbels, *J. Chem. Phys.* **136**, 044305 (2012).
8. A. F. Bierau, P. Kupser, G. Meijer, G. von Helden, *Phys. Rev. Lett.* **105**, 133402 (2010).
9. A. I. González-Flórez, D. –S. Ahn, S. Gewinner, W. Schöllkopf, G. von Helden, *Phys. Chem. Chem. Phys.* **17**, 21902 (2015).
10. E. Mucha, A. I. González-Flórez, M. Marianski, D. A. Thomas, W. Hoffmann, W. B. Struwe, H. S. Hahm, S. Gewinner, W. Schöllkopf, P. E. Seeberger, G. von Helden, K. Pagel, *Angew. Chem. Int. Ed.* **56**, 11248 (2017).
11. D. A. Thomas, E. Mucha, S. Gewinner, W. Schöllkopf, G. Meijer, G. von Helden, *J. Phys. Chem. Lett.* **9**, 2305 (2018).
12. M. Kuhn, M. Renzler, J. Postler, S. Ralser, S. Spieler, M. Simpson, H. Linnartz, A. G. G. M. Tielens, J. Cami, A. Mauracher, Y. Yang, M. Alcami, F. Martin, M. K. Beyer, R. Wester, A. Lindinger, P. Scheier, *Nat. Comm.* **7**, 13550 (2016).

13. S. Spieler, M. Kuhn, J. Postler, M. Simpson, R. Wester, P. Scheier, W. Ubachs, X. Bacalla, J. Bouwman, H. Linnartz, *Astrophys. J.* **846**, 168 (2017).
14. A. Kaiser, J. Postler, M. Ončák, M. Kuhn, M. Renzler, S. Spieler, M. Simpson, M. Gatchell, M. K. Beyer, R. Wester, F. Gianturco, P. Scheier, *J. Phys. Chem. Lett.* **9**, 1237 (2018).
15. J. A. Davies, N. A. Besley, S. Yang, A. M. Ellis, *J. Phys. Chem. Lett.* **10**, 2108 (2019).
16. E. J. Bieske, O. Dopfer, *Chem. Rev.* **100**, 3963 (2000).
17. O. Dopfer, *Int. Rev. Phys. Chem.* **22**, 437 (2003).
18. C. J. Johnson, A. B. Wolk, J. A. Fournier, E. N. Sullivan, G. H. Weddle, M. A. Johnson, *J. Chem. Phys.* **140**, 221101 (2014).
19. N. Heine, K. R. Asmis, *Int. Rev. Phys. Chem.* **34**, 1, (2015).
20. J. Roithova, A. Gray, E. Andris, J. Jasik, D. Gerlich, *Acc. Chem. Res.* **49**, 223 (2016).
21. D. Gerlich, *J. Chin. Chem. Soc.* **65**, 637 (2018).
22. H. Schwarz, K. R. Asmis, *Chem. Eur. J.* **25**, 2112 (2019).
23. N. M. Lakin, R. V. Olkhov, O. Dopfer, *Faraday Discuss.* **118**, 455 (2001).
24. P. J. Kelleher, C. J. Johnson, J. A. Fournier, M. A. Johnson, A. B. McCoy, *J. Phys. Chem. A*, **119**, 4170 (2015).
25. E. J. Bieske, A. M. Soliva, A. Freidmann, J. P. Maier, *J. Chem. Phys.* **96**, 28 (1992).
26. T. Amano, K. Tanaka, *J. Chem. Phys.* **83**, 3721 (1985).
27. O. Dopfer, R. V. Olkhov, D. Roth, J. P. Maier, *Chem. Phys. Lett.* **296**, 585 (1998).
28. J. Tang, Y. Xu, A. R. W. McKellar, W. Jäger, *Science* **297**, 2030 (2002).
29. A. R. W. McKellar, Y. Xu, W. Jäger, *Phys. Rev. Lett.* **97**, 183401 (2006).
30. A. R. W. McKellar, *J. Chem. Phys.* **128**, 044308 (2008).
31. A. R. W. McKellar, *J. Chem. Phys.* **127**, 044315 (2007).
32. J. Tandy, C. Feng, A. Boatwright, G. Sarma, A. M. Sadoon, A. Shirley, N. D. N. Rodrigues, E. M. Cunningham, S. Yang, A. M. Ellis, *J. Chem. Phys.* **144**, 121103 (2016).

33. A. M. Sadoon, G. Sarma, E. M. Cunningham, J. Tandy, M. W. D. Hanson-Heine, N. A. Besley, S. Yang, A. M. Ellis, *J. Phys. Chem. A* **120**, 8085 (2016).

34. M. I. Sulaiman, S. Yang, A. M. Ellis, *J. Phys. Chem. A* **121**, 771 (2017).

35. Gaussian 16, Revision B.01, M. J. Frisch, G. W. Trucks, H. B. Schlegel, G. E. Scuseria, M. A. Robb, J. R. Cheeseman, G. Scalmani, V. Barone, G. A. Petersson, H. Nakatsuji, X. Li, M. Caricato, A. V. Marenich, J. Bloino, B. G. Janesko, R. Gomperts, B. Mennucci, H. P. Hratchian, J. V. Ortiz, A. F. Izmaylov, J. L. Sonnenberg, D. Williams-Young, F. Ding, F. Lipparini, F. Egidi, J. Goings, B. Peng, A. Petrone, T. Henderson, D. Ranasinghe, V. G. Zakrzewski, J. Gao, N. Rega, G. Zheng, W. Liang, M. Hada, M. Ehara, K. Toyota, R. Fukuda, J. Hasegawa, M. Ishida, T. Nakajima, Y. Honda, O. Kitao, H. Nakai, T. Vreven, K. Throssell, J. A. Montgomery, Jr., J. E. Peralta, F. Ogliaro, M. J. Bearpark, J. J. Heyd, E. N. Brothers, K. N. Kudin, V. N. Staroverov, T. A. Keith, R. Kobayashi, J. Normand, K. Raghavachari, A. P. Rendell, J. C. Burant, S. S. Iyengar, J. Tomasi, M. Cossi, J. M. Millam, M. Klene, C. Adamo, R. Cammi, J. W. Ochterski, R. L. Martin, K. Morokuma, O. Farkas, J. B. Foresman, and D. J. Fox, Gaussian, Inc., Wallingford CT, 2016.

36. J. A. Davies, M. W. Hanson-Heine, N. A. Besley, A. Shirley, J. Trowers, S. Yang, A. M. Ellis, *Phys. Chem. Chem. Phys.* **21**, 13950 (2019).

37. PGOPHER version 10.1, C. M. Western, 2018, University of Bristol Research Data Repository, doi:10.5523/bris.3mqfb4glgkr8a2rev7f73t300c.

38. C. M. Western, *J. Quant. Spectrosc. Rad. Transfer* **186**, 221 (2016).

39. W. K. Lewis, B. E. Applegate, J. Sztaray, B. Sztaray, T. Baer, R. J. Beamish, R. E. Miller, *J. Am. Chem. Soc.* **126**, 11283 (2004).

40. W. K. Lewis, R. J. Beamish, R. E. Miller, *J. Chem. Phys.* **123**, 141103 (2005).

41. K. Nauta, R. E. Miller, *Science* **287**, 293 (2000).

42. K. Nauta, R. E. Miller, *Science* **283**, 1895 (1999).

43. J. D. Pickering, B. Shepperson, L. Christiansen, H. Staplefeld, *J. Chem. Phys.* **149**, 154306 (2018).
44. S. A. Nizkorodov, O. Dopfer, T. Ruchti, J. P. Maier, E. J. Bieske, *J. Phys. Chem.* **99**, 17118 (1995).
45. G. E. Douberly, A. M. Ricks, B. W. Ticknor, M. A. Duncan, *J. Phys. Chem. A* **112**, 950 (2008).
46. H. Li, Y.-T. Ma, *J. Chem. Phys.* **137**, 234310 (2012).
47. F. Uhl, D. Marx, *Angew. Chem. Int. Ed.* **57**, 14792 (2018).
48. C. M. Breneman and K. B. Wiberg, *J. Comp. Chem.* **11**, 361 (1990).

The Journal of Chemical Physics

PLEASE CITE THIS ARTICLE AS DOI: 10.1063/1.5124137

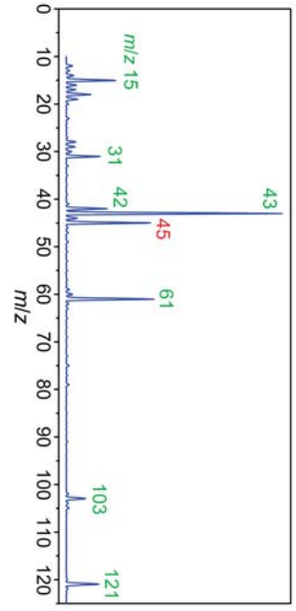

PLEASE CITE THIS ARTICLE AS DOI: 10.1063/1.5124137

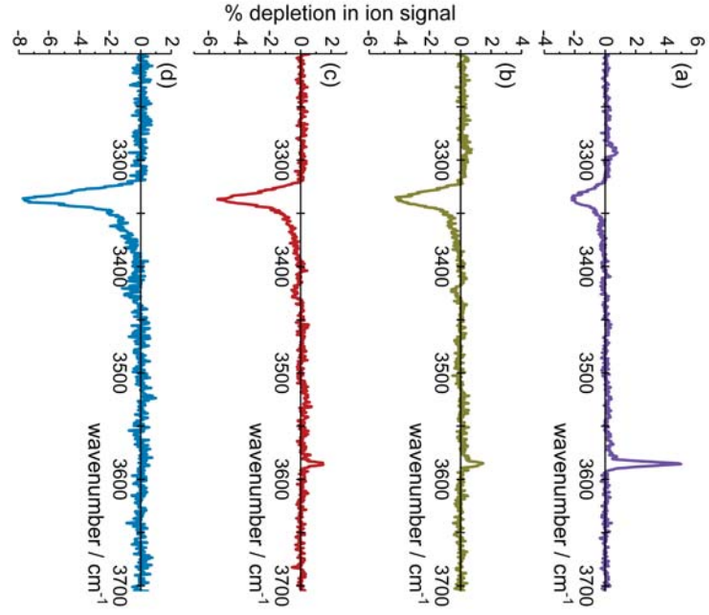

PLEASE CITE THIS ARTICLE AS DOI: 10.1063/1.5124137

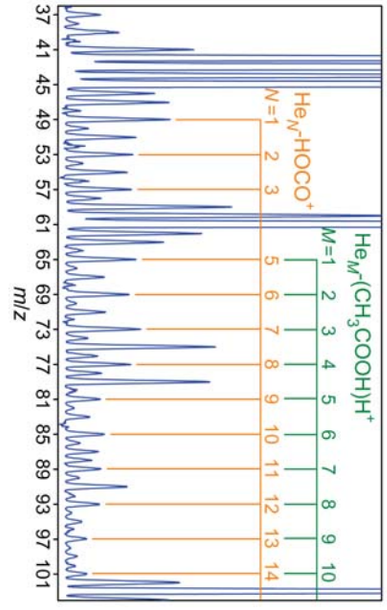

PLEASE CITE THIS ARTICLE AS DOI: 10.1063/1.5124137

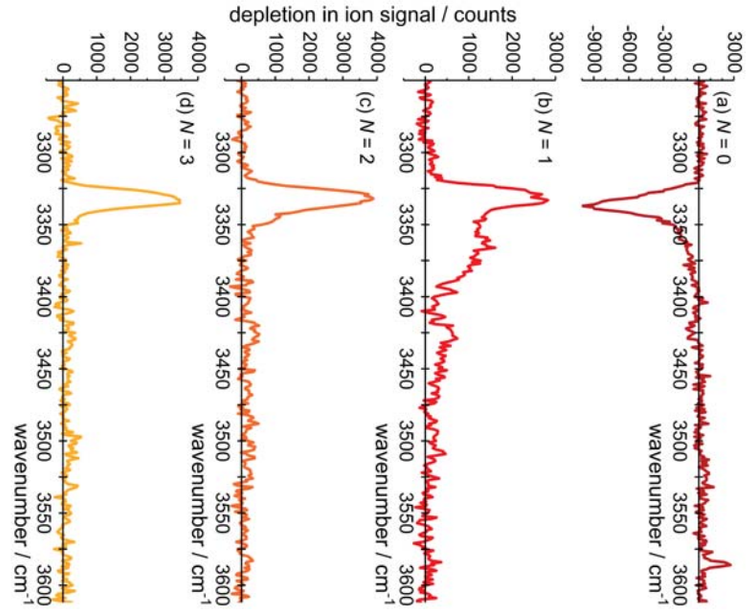

PLEASE CITE THIS ARTICLE AS DOI: 10.1063/1.5124137

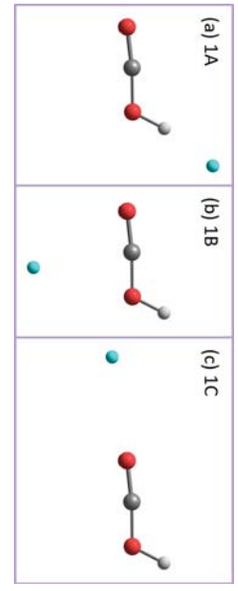

AIP Publishing

The Journal of Chemical Physics

ACCEPTED MANUSCRIPT

This is the author's peer reviewed, accepted manuscript. However, the online version of record will be different from this version once it has been copyedited and typeset.
PLEASE CITE THIS ARTICLE AS DOI: 10.1063/1.5124137

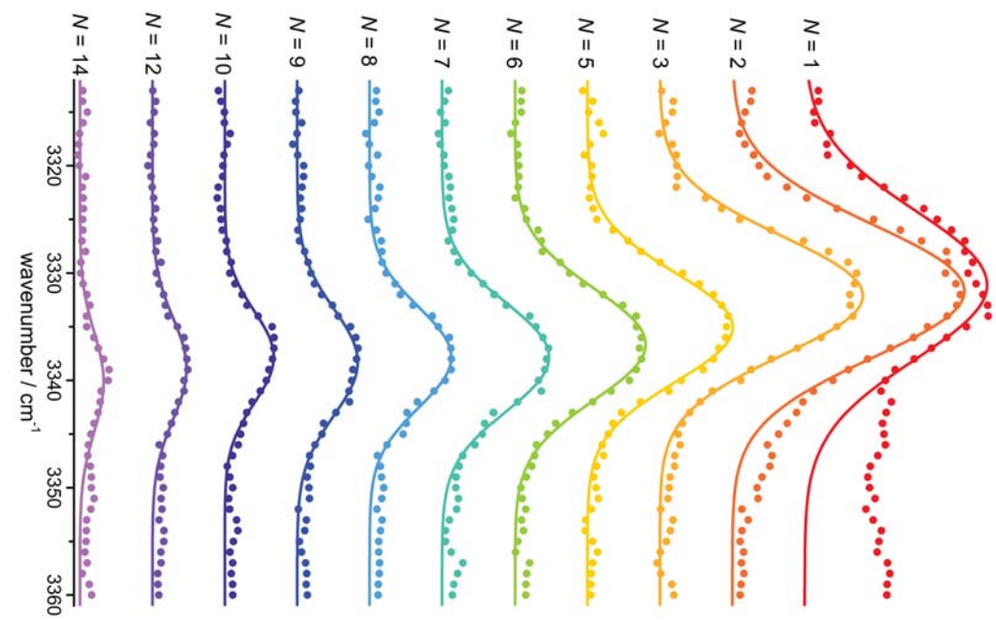

PLEASE CITE THIS ARTICLE AS DOI: 10.1063/1.5124137

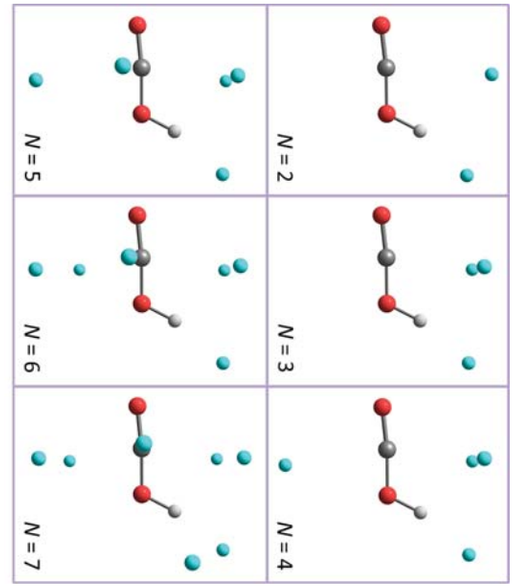

PLEASE CITE THIS ARTICLE AS DOI: 10.1063/1.5124137

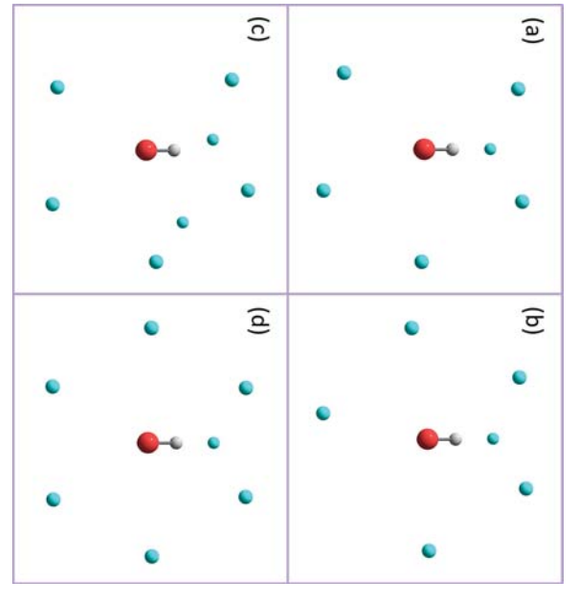

AIP Publishing

The Journal of Chemical Physics

ACCEPTED MANUSCRIPT

PLEASE CITE THIS ARTICLE AS DOI: 10.1063/1.5124137